

BGD

11, 4857–4908, 2014

**Remotely sensed
land-surface energy
fluxes**

R. Guzinski et al.

Remotely sensed land-surface energy fluxes at sub-field scale in heterogeneous agricultural landscape and coniferous plantation

R. Guzinski¹, H. Nieto¹, R. Jensen¹, and G. Mendiguren^{1,2}

¹Department of Geosciences and Natural Resource Management, University of Copenhagen, Oster Voldgade 10, 1350 Copenhagen K, Denmark

²Instituto de Economía, Geografía y Demografía. Centro de Ciencias Humanas y Sociales, Consejo Superior de Investigaciones Científicas (CSIC), Albasanz 26–28, 28037, Madrid, Spain

Received: 3 February 2014 – Accepted: 18 March 2014 – Published: 28 March 2014

Correspondence to: R. Guzinski (rag@ign.ku.dk)

Published by Copernicus Publications on behalf of the European Geosciences Union.

Title Page

Abstract

Introduction

Conclusions

References

Tables

Figures

◀

▶

◀

▶

Back

Close

Full Screen / Esc

Printer-friendly Version

Interactive Discussion



Abstract

In this study we evaluate a methodology for disaggregating land surface energy fluxes estimated with the Dual Time Difference (DTD) model which uses the day and night polar orbiting satellites observations of Land Surface Temperature (LST) as a remotely sensed input. The DTD model is run with MODIS input data at a spatial resolution of around 1 km while the disaggregation uses Landsat observations of LST to produce fluxes at a nominal spatial resolution of 30 m. The higher resolution modeled fluxes can be directly compared against eddy-covariance based flux tower measurements to ensure more accurate model validation and also provide a better visualization of fluxes' spatial patterns in heterogeneous areas allowing for development of, for example, more efficient irrigation practices. The disaggregation technique is evaluated in an area covered by the Danish Hydrological Observatory (HOBE), in the west of the Jutland peninsula, and the modeled fluxes are compared against measurements from two flux towers: first one in a heterogeneous agricultural landscape and second one in a homogeneous conifer plantation. The results indicate that the disaggregated fluxes have greatly improved accuracy as compared to high resolution fluxes derived directly with Landsat data without the disaggregation. At the agricultural site the disaggregated fluxes display negligible bias and almost perfect correlation ($r > 0.90$) with Eddy Covariance based measurements, while at the plantation site the results are encouraging but not ideal. In addition we introduce a modification to the DTD model by replacing the "parallel" configuration of the resistances to sensible heat exchange by the "series" configuration. The later takes into account the in-canopy air temperature and substantially improves the accuracy of the DTD model.

BGD

11, 4857–4908, 2014

Remotely sensed land-surface energy fluxes

R. Guzinski et al.

Title Page

Abstract

Introduction

Conclusions

References

Tables

Figures



Back

Close

Full Screen / Esc

Printer-friendly Version

Interactive Discussion



1 Introduction

Reliably estimating surface energy fluxes (latent heat – LE, sensible heat – H , ground heat – G , and net radiation – R_n) in agricultural landscapes requires the model spatial resolution to match the dominant landscape feature scale (Kustas and Albertson, 2003; Kustas et al., 2004). Since most of the models require satellite observations, particularly of land surface temperature (LST), for operational use over larger areas, their spatial resolution is limited by the resolution of those satellite observations. In many heterogeneous agricultural landscapes the field sizes can be on order of a couple hectares meaning that the spatial resolution of the LST satellite observation needs to be on the order of 100 m \times 100 m. Among the few satellites which can provide this information on regular basis is the Landsat satellite family with LST resolution of 120/60 m, resampled by the data provider to 30 m (http://landsat.usgs.gov/band_designations_landsat_satellites.php, last accessed 17 March 2014). There are a number of methodologies which can exploit the Landsat derived LST for estimating surface energy fluxes. They range from empirical ones, like the triangle approach (Stisen et al., 2008), to more physically based ones, such as one source (Bastiaanssen et al., 1998) or two source (Norman et al., 1995) energy balance models. The empirical methods suffer limitations due to simple assumptions and ratios employed within the models, while the physically based models are highly sensitive to errors in the LST measurements (Anderson et al., 1997). This is particularly important when using Landsat LST estimates, since they are derived from only one thermal band and so are highly susceptible to atmospheric water vapor absorption (Sobrino et al., 2004). Although the new Landsat 8 satellite has two thermal bands it is recommended to refrain from using one of them for LST estimation (USGS, http://landsat.usgs.gov/calibration_notices.php, last accessed 14 January 2014). Li et al. (2004) have estimated LST using the older Landsat 5 and Landsat 7 satellites and obtained a mean absolute difference of between 1 °C and 1.5 °C when compared to tower based brightness temperature measurements.

BGD

11, 4857–4908, 2014

Remotely sensed land-surface energy fluxes

R. Guzinski et al.

Title Page

Abstract

Introduction

Conclusions

References

Tables

Figures



Back

Close

Full Screen / Esc

Printer-friendly Version

Interactive Discussion



Remotely sensed land-surface energy fluxes

R. Guzinski et al.

Title Page

Abstract

Introduction

Conclusions

References

Tables

Figures



Back

Close

Full Screen / Esc

Printer-friendly Version

Interactive Discussion



To overcome issues arising from uncertainty in absolute temperature measurements, either of satellite LST or air temperature from models or remotely located meteorological stations, the more robust Two Source Energy Balance (TSEB) modeling scheme based models, such as ALEXI (Anderson et al., 1997) or Dual-Temperature-Difference (DTD) (Norman et al., 2000), make use of temperature difference between early morning and late morning or early afternoon measurements. Both models require LST estimates provided by geostationary satellites, due to their high temporal resolution, and therefore produce flux estimates at low spatial resolution of around 5 km. The ALEXI model has previously been coupled to the DisALEXI disaggregation algorithm (Anderson et al., 2004), allowing the fluxes estimated at the geostationary satellite spatial resolution to be disaggregated using a Landsat LST observation to Landsat spatial scale while preserving the advantages provided by using the differential temperature measurements. This allows the ALEXI modeled fluxes to be directly compared against eddy-covariance based flux tower measurements, which have a measurement footprint that ranges from tens to hundreds of meters away from the tower and is constantly changing depending on wind speed and direction, atmospheric stability and surface roughness. It also provides a better visualization of fluxes' spatial patterns in heterogeneous areas, such as typical agricultural landscapes, allowing for monitoring of individual fields and development of, for example, more efficient irrigation practices (Anderson et al., 2011).

More recently a modification of the DTD model has been developed to allow the use of LST derived by polar orbiting satellites with night-time and day-time overpass times (Guzinski et al., 2013). This was done by exploiting the day and night LST measurements provided by the MODIS sensor on board of the Aqua and Terra satellites and by replacing the early morning temperature measurement in the DTD model with one taken at night by the Aqua satellite. By using the data provided by polar orbiting satellites the geographical region of the applicability of the DTD model has been extended to areas at high latitudes, such as Scandinavia, which cannot be reliably monitored with geostationary satellites due to severe geometric and atmospheric effects. The modified

DTD model was run with the LST estimates provided by the MODIS sensor aboard the Terra and Aqua satellites and compared to flux tower observations in a number of ecosystems, in most cases obtaining satisfactory results.

However, one site where the modified DTD model did not perform satisfactorily was the Voulund (VOU) agricultural site in western Denmark. A possible factor contributing to the poor performance of the model at this particular location is the highly heterogeneous nature of the site (Guzinski et al., 2013). Figure 1a shows the orthophoto of the VOU site, with the overlaid grid indicating the location of MODIS pixels in the MODIS sinusoidal projection. Within each 930 m MODIS pixel there are a number agricultural fields present, each one at a different stage of crop development, as well as shrubs and small plantations of young spruce and fir. The LST contrast within the MODIS pixel, caused by heterogeneity, should not have such a large influence on the modeled fluxes, especially for estimates which are not at the extremes of the distribution (Norman et al., 2003). Therefore we hypothesize that the discrepancy between the modeled and measured fluxes is in a large measure due to the mismatch between the footprint of the flux tower measurements and the flux footprint of the MODIS pixel. In addition, as the dominant wind direction is from the west, a large part of the flux tower footprint lies in the MODIS pixel adjacent to the one containing the flux tower.

To test the hypothesis our objective was to develop a DTD disaggregation algorithm, based on DisALEXI (Anderson et al., 2004), using high resolution observations from the Landsat family of satellites. This disaggregation methodology has not been previously applied to fluxes derived with the DTD model or fluxes derived purely with polar orbiting satellites. We tested the disaggregation at two different sites, the agricultural site mentioned previously (VOU) as well as a conifer plantation Gludsted (GLU), which on the contrary to VOU is homogeneous at MODIS pixel scale but with certain heterogeneity at a smaller spatial scale (Fig. 1b). At both sites we tested the robustness of the disaggregation algorithm by comparing it to fluxes estimated by running the TSEB model directly with Landsat data without performing the disaggregation. In addition, we also modified the DTD formulation to enable interaction between the modeled canopy

BGD

11, 4857–4908, 2014

Remotely sensed land-surface energy fluxes

R. Guzinski et al.

Title Page

Abstract

Introduction

Conclusions

References

Tables

Figures



Back

Close

Full Screen / Esc

Printer-friendly Version

Interactive Discussion



and soil fluxes, which has a significant impact on the accuracy of the model, and tested the performance of the model when used with modeled, instead of in situ, meteorological data for operational applications at regional scales.

In Sect. 2 we present the data used in this study: the validation fluxes and meteorological observations from the VOU and GLU tower based measurements, satellite based inputs and modeled meteorological data. Section 3 explains the principles behind the TSEB and DTD models and the disaggregation algorithm used in this study, with the actual model equations presented in the Appendices A1 and A2. In Sect. 4 we first compare the performance of the DTD model at MODIS pixel scale with the old and new model formulations. Then, we evaluate the disaggregated high resolution fluxes and compare them with fluxes obtained by using Landsat data directly with TSEB without disaggregation and the low resolution DTD fluxes. This is done using both locally measured and modeled meteorological inputs. We conclude the discussion in Sect. 5.

2 Data

2.1 Flux tower data

The models were run over an area covering the measurement footprints of two eddy covariance (EC) flux towers located on Jutland peninsula in western Denmark (Fig. 1). The first flux tower is placed in a highly heterogeneous agricultural site, Voulund (VOU), while the second is in a coniferous plantation, Gludsted (GLU), dominated by *Picea abies* with an average height of 20 m and homogeneous at MODIS spatial resolution while displaying small scale heterogeneity due to forest roads and clearings and stands of different species and ages (Ringgaard et al., 2012). Both the sites are in sandy soils with temperate maritime climate experiencing mean annual precipitation of 990 mm and mean annual temperature of 8.2°C. The two ecosystems encompassed by the VOU and GLU flux tower sites together represent around 85 % of land cover type of the

BGD

11, 4857–4908, 2014

Remotely sensed land-surface energy fluxes

R. Guzinski et al.

Title Page

Abstract

Introduction

Conclusions

References

Tables

Figures



Back

Close

Full Screen / Esc

Printer-friendly Version

Interactive Discussion



Skjern river catchment, which is the largest river in Denmark in terms of water volume. A more detailed description of the sites is presented in Ringgaard et al. (2011).

Both sites were equipped with a Gill R3-50 sonic anemometer (Gill Instruments Ltd., Lymington, UK) and LI-7500 open-path infrared gas analyzer (IRGA) (Li-Cor Inc., Lincoln, NE, USA) to continuously measure wind components in three dimensions and concentrations of water vapor, sensible heat, and CO₂. The EC system at VOU is mounted at a height of 6 m and air temperature is measured at 4 m above ground, while at GLU the EC system is 38 m a.g.l. and air temperature is measured at 30 m above ground. Turbulent fluxes were calculated using the EddyPro 4.2 software (Li-Cor Inc., Lincoln, NE, USA). The routine to calculate the fluxes includes, coordinate rotation, block averaging (30 min windows), corrections for density fluctuations (Webb et al., 1980), and spectral corrections (Moncrieff et al., 1997). Additionally, the fluxes were corrected for surface heating of the IRGA (Burba et al., 2008), which has a most pronounced effect during cold season. Fluxes were quality checked according to Mauder and Foken (2006) and flagged if quality criteria were not met. The only setting that were different between the two sites were the coordinate rotation. At VOU, where canopy height and structure changes during the season, and where the canopy is nearly homogeneous in all directions, double rotation was applied. At GLU, where the lined structure of the trees could potentially cause flow distortions in specific directions the planar fit method (Wilczak et al., 2001) was applied. Processed data were subjected to a further quality control to detect outliers in the calculated 30 min average fluxes according to the method proposed in Papale et al. (2006). As some data were rejected in the quality control, there are gaps in the dataset. Gaps are filled by the standardized method proposed by Reichstein et al. (2005) with the online tool available at <http://www.bgc-jena.mpg.de/bgi/index.php/Services/REddyProcWeb> (last accessed 10 January 2014).

Both towers also have sensor for measuring the four components of net radiation, incoming/outgoing and shortwave/longwave, as well as air temperature and humidity. The 30 min averaged air temperature, wind speed, humidity and incoming solar radia-

BGD

11, 4857–4908, 2014

Remotely sensed land-surface energy fluxes

R. Guzinski et al.

Title Page

Abstract

Introduction

Conclusions

References

Tables

Figures

◀

▶

◀

▶

Back

Close

Full Screen / Esc

Printer-friendly Version

Interactive Discussion



tion observations from the towers were used as input for the DTD and TSEB models. During the validation of the model performance only the measured, not gap filled, fluxes were used. Energy closure in the measured fluxes was ensured by assigning residual energy to the latent heat, based on the assumption that errors in the measurements of LE are larger than in the measurements of H due to the nature of the sensors and the fluxes (Foken et al., 2011). In addition at sites where Bowen Ratio (BR) is low, such as VOU, it is recommended to assign the residual energy to LE (Kustas et al., 2012), while at high flux towers, such as at GLU, the 30 min averaging period can miss the low frequency eddies which, once again, affects mostly LE (Finnigan et al., 2003).

2.2 Satellite data

MODIS data used as input for the DTD algorithm is presented in Guzinski et al. (2013). Briefly, M*D11A1 V5 daily product (Wan, 2006) from Aqua and Terra satellites was used for LST and emissivity estimations, with the night time observations taken from Aqua overpass around 1 a.m. local time and day time observations taken from Aqua, Terra or both satellites (resulting in two flux estimates per day) depending on the quality of the observations. LST observations with all View Zenith Angles (VZA), up to 65° , were used. Other MODIS products used are 4 day MCD15A3 for Leaf Area Index (LAI) (Knyazikhi et al., 1999), 16 day MOD13A2 for vegetation indices required for estimating the fraction of vegetation that is green (Guzinski et al., 2013) and 8 day MCD43B3 product for albedo.

Landsat data came from all cloud free observations taken by Landsat 5, Landsat 7 and Landsat 8 over the period 2009 till 2013 over the study area with the spatial resolution in the visible/near-infrared part of the spectrum of 30 m and thermal infrared observations resampled to 30 m by the data provider (USGS, http://landsat.usgs.gov/band_designations_landsat_satellites.php, last accessed 17 January 2014). An atmospheric correction was performed with MODTRAN 5 (Berk et al., 2006) with the standard mid-latitude summer atmospheric profile used for all of the atmospheric parameters except for the total column water vapor, ozone, atmospheric optical thickness and temperature

Remotely sensed land-surface energy fluxes

R. Guzinski et al.

Title Page

Abstract

Introduction

Conclusions

References

Tables

Figures



Back

Close

Full Screen / Esc

Printer-friendly Version

Interactive Discussion



Remotely sensed land-surface energy fluxes

R. Guzinski et al.

Title Page

Abstract

Introduction

Conclusions

References

Tables

Figures



Back

Close

Full Screen / Esc

Printer-friendly Version

Interactive Discussion



and pressure profiles which came from the daily Terra MOD08 gridded atmospheric product. The top-of-canopy reflectances in the visible and near infrared parts of the spectrum were derived following the approach of Xu et al. (2008) which is based on FLAASH (Anderson et al., 2002) with the adjacency effect considered to be significant in an area with a diameter of 1 km (Verhoef and Bach, 2003). Cloud masking was performed using the Fmask algorithm (Zhu and Woodcock, 2012), modified to also work with Landsat 8 bands assuming that Landsat 8 sensor has the same characteristics as Landsat 7 sensor.

The vegetation indices used in TSEB were calculated directly from the top-of-canopy reflectances of the appropriate Landsat bands. LAI and albedo for Landsat were derived using decision tree regression trained with high quality MODIS LAI and albedo observations and Landsat reflectances, from all the VIS and NIR bands, aggregated to MODIS pixel size (Gao et al., 2012). Emissivity was linear scaled with fractional vegetation cover obtained from NDVI (Stisen et al., 2007). Bare soil emissivity was set to 0.950 at NDVI of 0.15 and full vegetation cover emissivity was set to 0.995 at NDVI of 0.70. Landsat LST was estimated using the approach of Coll et al. (2010) with the upwelling atmospheric radiance and atmospheric transmittance obtained from a MODTRAN run with the simulated sensor at satellite height and, LST of 0 K and ground emissivity of 1 (albedo of 0) and the downwelling atmospheric radiance from a MODTRAN run with the sensor just above the surface and ground emissivity of 0 (albedo of 1). Finally, land cover classification was taken from the 2006 update of the Corine land cover.

2.3 Modeled meteorological data

To determine regional scale surface energy fluxes the local, tower based, meteorological observations need to be replaced by an interpolated or modeled meteorological dataset. Therefore we have also tested the performance of the disaggregation algorithm when such data is being used. The modeled meteorological data came from the ERA-Interim reanalysis dataset (Dee et al., 2011) provided by the European Centre

for Medium-Range Weather Forecasts (ECMWF). The products used were the 2 m air temperature (2T), 2 m dew point temperature (2D) used to calculate the vapor pressure, the 10 m horizontal wind speed (10U and 10V) and surface solar radiation downward (SSRD). Although the air temperature field is nominally at 2 m height, in the model it was assumed that it is the air temperature measured at 100 m above the ground. This can be justified based on the fact that the air temperature is modeled at very low spatial resolution indicating that it can be treated as blending height temperature. In addition the time differential nature of DTD removes any biases caused by increasing the temperature measurement height. The wind field was assumed to be at 10 m above the canopy, or the ground if the canopy is shorter than 10 m. The data is provided at a 0.75° spatial resolution and was subsetted and resampled into a MODIS sinusoidal grid projection for the MODIS tile covering the area of interest. In the temporal domain the data was linearly interpolated between the 3 hourly observation or modeled timesteps.

3 Methods

3.1 TSEB

The Two Source Energy Balance (TSEB) model was developed by Norman et al. (1995) and later underwent a number of modifications (e.g. Kustas and Norman, 1999). The main innovation in the TSEB model is to split the LST observed at view zenith angle (VZA) θ , $T_R(\theta)$, into vegetation canopy and soil temperatures, T_C and T_S respectively, based on the fraction of view of the radiometer covered by vegetation, $f(\theta)$, which is estimated from observation geometry and the fraction of vegetation canopy cover:

$$T_R(\theta) \approx (f(\theta)T_C^4 + (1 - f(\theta))T_S^4)^{0.25} \quad (1)$$

This allows the sensible heat fluxes from the vegetation and soil to be computed separately, based on the temperature gradient from the canopy and soil respectively and air

BGD

11, 4857–4908, 2014

Remotely sensed land-surface energy fluxes

R. Guzinski et al.

Title Page

Abstract

Introduction

Conclusions

References

Tables

Figures

◀

▶

◀

▶

Back

Close

Full Screen / Esc

Printer-friendly Version

Interactive Discussion



temperature at some height above or within the canopy. The latent heat flux from the canopy is initially estimated using a modified Priestly–Taylor approximation (Priestley and Taylor, 1972), while the latent heat flux from the soil is estimated as a residual of the other fluxes thus ensuring energy balance closure. The TSEB model is used in this study for disaggregating fluxes from low to high spatial resolutions as well as for directly estimating fluxes with Landsat data. The equations used in the current implementation of the TSEB model are presented in Appendix A1.

3.2 DTD

One of the limitations of thermal-based energy balance models, including the TSEB model, is their sensitivity to the temperature gradient between the LST (or its soil and canopy components) and the air temperature. This makes them highly susceptible to errors introduced in the absolute measurements of LST or air temperature. To improve the robustness of the TSEB modeling scheme two approaches, ALEXI (Anderson et al., 1997) and DTD (Norman et al., 2000), have been developed which replace the absolute temperature estimates by time-differential temperature measurement between a time early in the morning and another time later during the day. ALEXI couples surface energy balance to a model of atmospheric boundary layer growth during the morning hours and requires an atmospheric profile sounding during the early morning hours, while DTD implements a simpler model formulation requiring the same inputs as TSEB but at the two observation times. Both ALEXI and DTD models require the first temperature measurement one hour past sunrise, when surface heat fluxes are minimal (Anderson et al., 1997). This means that they require precise timing of the morning observation and so are dependent on measurements coming from geostationary satellites with their sub-hourly temporal resolution.

Guzinski et al. (2013) have established that it is possible to replace the early morning temperature observation in the DTD model with night-time observations with minimal degradation in the retrieved fluxes. They have also introduced modifications to the model to accommodate the two LST observations having different VZA's thus allow-

Remotely sensed land-surface energy fluxes

R. Guzinski et al.

[Title Page](#)

[Abstract](#)

[Introduction](#)

[Conclusions](#)

[References](#)

[Tables](#)

[Figures](#)



[Back](#)

[Close](#)

[Full Screen / Esc](#)

[Printer-friendly Version](#)

[Interactive Discussion](#)



ing the use of DTD with polar orbiting satellites which take observation over the area of interest during a night-time and day-time overpasses. Another modification of the DTD model, presented in this paper, is to use “series” resistance network instead of a “parallel” one for the calculation of the sensible heat fluxes. The advantage of the “series” resistance network is that it takes into account the interaction between the fluxes coming from the canopy and the soil by estimating the in-canopy air temperature. The differences between the two resistance network configurations are presented in Norman et al. (1995) while the modification to the DTD model, together with other implementation details, is shown in Appendix A2. This modified DTD model is used in this study to estimate the coarse resolution fluxes.

3.3 Disaggregation

The disaggregation methodology is based on DisALEXI algorithm, developed for disaggregating fluxes derived with the ALEXI model (Norman et al., 2003). Since ALEXI requires geostationary observations as input it produces flux estimates with a nominal pixel resolution of 5 km. Another output of ALEXI is the air temperature at blending height, assumed to be 50 m above the surface, also at 5 km resolution (Anderson et al., 1997). During the disaggregation procedure this air temperature is used as an upper boundary condition, while LST derived with high resolution sensor (such as Landsat) is bias corrected to match the LST used as input to ALEXI at 5 km scale and then used as the lower boundary condition for a TSEB model (see Fig. 1 in Norman et al., 2003). This ensures that the surface-air temperature gradient, and therefore the surface fluxes, are consistent between the lower resolution ALEXI estimates and the higher resolution TSEB ones. One of the assumptions of DisALEXI is that the temperature at blending height is constant within the 5 km pixel. This assumption might not necessary hold in highly heterogeneous landscapes (Anderson et al., 2004; Kustas and Albertson, 2003). However, in this application we are disaggregating from 1 km MODIS pixels which means that the assumption has a better chance of being met than if 5 km pixels were used.

Remotely sensed land-surface energy fluxes

R. Guzinski et al.

Title Page

Abstract

Introduction

Conclusions

References

Tables

Figures



Back

Close

Full Screen / Esc

Printer-friendly Version

Interactive Discussion



Remotely sensed land-surface energy fluxes

R. Guzinski et al.

Title Page

Abstract

Introduction

Conclusions

References

Tables

Figures

⏪

⏩

◀

▶

Back

Close

Full Screen / Esc

Printer-friendly Version

Interactive Discussion



In a recent application of DisALEXI the consistency between the low resolution and high resolution model runs was ensured using the daily H estimates, up-scaled from the instantaneous H estimates provided by ALEXI and the higher resolution TSEB model using the assumption of self-preservation of evaporative fraction (EF) (Cammalleri et al., 2013a). This removes the requirement of having the low and high resolution flux estimates congruent in time and allows the technique to be used with polar orbiting satellites with different overpass times. In this approach the ALEXI derived blending height temperature is used as the initial value for the upper boundary condition of the high resolution TSEB run and is then iteratively adjusted until the daily H estimates with ALEXI and TSEB, aggregated to ALEXI pixel size, match.

There is no general agreement on the best way to upscale instantaneous fluxes to daily values, or, in the current application, to compare two instantaneous flux measurements taken at different times of the same day while removing their time dependent component. Some recent studies suggest that EF remains stable, especially around noon hours in cloud free condition, in a wide range of ecosystems (Peng et al., 2013) while others have proposed the replacement of EF with the ratio of LE to incoming solar radiation at ground level (Cammalleri et al., 2013b). Therefore in this study we evaluate three approaches to estimate what we term the constant ratio (CR): EF, ratio of LE to incoming solar radiation, $LE/R_{s, in}$, and the ratio of H to incoming solar radiation, $H/R_{s, in}$. The third approach is included since the values of LE and H used for calculating the CR come from the DTD and TSEB model outputs. Therefore it can be assumed that the estimated value of H will be more accurate than LE as it is estimated directly while LE is estimated as residual of the other fluxes.

In summary the disaggregation method is as follows:

1. Estimates of fluxes at MODIS pixel scale are provided by running DTD with MODIS inputs.
2. For each MODIS pixel the constant ratio, assumed to remain constant during the daylight hours, is calculated using the DTD output fluxes.

cantly reduced with the “series” formulation. A large decrease in correlation, especially at GLU, is caused by the model forcing the latent heat flux to be zero when negative daytime evapotranspiration values are obtained at the end of the calculation (see Appendices). Those fluxes, and the associated sensible heat fluxes, can be easily flagged and removed from the results if desired thus increasing the overall accuracy and correlation of the remaining modeled fluxes.

Since the “series” version of the DTD model provides substantial improvements it is the version that is used in the remainder of this study.

4.2 Disaggregation at the agricultural site – VOU

The DTD model was run at the native MODIS resolution of 930 m over the VOU site using MODIS data and tower-based meteorological observations as input and the results were disaggregated to 30 m resolution using the TSEB model with Landsat data and tower-based meteorological observations as input. All the dates between 2009–2013 when high quality, cloud free MODIS and Landsat observations were available were considered. Figure 3 shows the comparison between the modeled sensible heat fluxes, aggregated to the estimated flux tower footprint, and the 30 min EC-based sensible heat flux measurements. The results for the three methods of estimating the CR ratio are presented (Fig. 3a–c) together with the fluxes estimated purely with DTD without disaggregation (Fig. 3e). The later fluxes are not aggregated to the flux tower footprint but instead the value of the MODIS pixel containing the flux tower is used. Statistical comparison is presented in Table 2.

The results are split into two sets. The first set (called S75) includes all the dates on which the disaggregation was successfully performed and Landsat pixels containing at least 75 % of the flux footprint weights are present but there is still some missing Landsat data. For dates when pixels representing less than 100 % of flux footprint weight are present the aggregated flux is scaled by the fraction of the missing footprint. The second set (called S100) is a subset of S75 and includes just the dates when there were no missing Landsat pixels within the MODIS pixels. The missing Landsat

Remotely sensed land-surface energy fluxes

R. Guzinski et al.

Title Page

Abstract

Introduction

Conclusions

References

Tables

Figures



Back

Close

Full Screen / Esc

Printer-friendly Version

Interactive Discussion



Remotely sensed land-surface energy fluxes

R. Guzinski et al.

Title Page

Abstract

Introduction

Conclusions

References

Tables

Figures

⏪

⏩

◀

▶

Back

Close

Full Screen / Esc

Printer-friendly Version

Interactive Discussion



pixels are most frequently caused by the faulty sensor aboard Landsat 7 satellite but can also be caused by clouds smaller than the MODIS pixel size (Fig. 4). In both cases the missing pixels can cause biases during the disaggregation procedure, especially if they are over an area with flux values significantly different than the mean MODIS pixel value, such as over an irrigated field surrounded by drier shrub-land. This is because the high resolution CR aggregated to a MODIS pixel has to match the MODIS CR even if there are some high resolution pixels missing within the MODIS pixel footprint.

The results in Table 2 show that there is substantial reduction in both bias and RMSE and increase in correlation when the fluxes are disaggregated, using all the three methods for estimating CR, when compared to the DTD fluxes. This is true for dates both in S75 and S100, however the disaggregation particularly reduces the errors for dates in S100 where RMSE is halved from 72 W m^{-2} in case of MODIS scale fluxes to between 32 W m^{-2} and 39 W m^{-2} in case of disaggregated fluxes. The bias changes sign and is reduced in magnitude from 26 W m^{-2} to between -5 W m^{-2} and -14 W m^{-2} depending on which disaggregation method is used while correlation between the observed and modeled fluxes is improved in all cases.

The differences between the three disaggregation methods are not very pronounced. However, the EF method of estimating CR used during the disaggregation is performing better than both $LE/R_{s, \text{in}}$ and $H/R_{s, \text{in}}$ according to all the statistical parameters with the exception of bias, with RMSE of 32 W m^{-2} and correlation coefficient of 0.94 for the S100 dataset. The three methods also displayed similar sensitivity to missing Landsat pixels with RMSE of S75 dataset being about double that of S100 and correlation coefficient decreasing by about a third. The bias is smaller in the S75 dataset.

To evaluate whether using the low resolution fluxes to establish boundary conditions for high resolution fluxes actually improves the high resolution model performance, the TSEB model was also run with air temperature taken directly from tower measurements and not adjusted based on the CR. In those cases the height of temperature measurements was set to 4 m which is the height of the tower based temperature sensor. The results are presented in Fig. 3d and in column ND_H of Table 2. There are less points

in panel (d) of Fig. 3 since the other panels often show two flux estimates per day: one taken with daytime Aqua satellite observation and the other one with the daytime Terra satellite observation. However, there is at most one Landsat observation per day. When dates in S75 are considered the RMSE and magnitude of bias obtained while running TSEB directly without disaggregation are larger than the ones obtained with the disaggregation algorithms, although correlation coefficient is higher. However, when just S100 set is considered the disaggregated fluxes perform much better than when high resolution TSEB is run directly. The RMSE is almost halved in the disaggregated fluxes while correlation is also improved.

4.3 Disaggregation at coniferous plantation – GLU

The DTD model and the three variants of the disaggregation algorithm were run over the GLU site in a similar fashion to VOI. The results are presented in Fig. 5 and Table 3. In case of GLU the disaggregation does not improve the accuracy of the modeled sensible heat flux when compared to the MODIS scale estimates. This was partially expected since the area around the tower is quite homogeneous at MODIS scale. For the S75 dataset the RMSE of low resolution fluxes (125 W m^{-2}) was among the range of RMSE of the disaggregated fluxes (from 107 W m^{-2} to 131 W m^{-2}). The same is true for correlation coefficient, having a value of 0.40 for low resolution fluxes and between 0.38 and 0.49 for the disaggregated fluxes, while the bias changed from positive to negative and decreased up to four times during the disaggregation. When just the S100 dataset is considered, the disaggregation reduces the accuracy of the model slightly. This is surprising since the low resolution fluxes in the S100 have very similar RMSE and lower bias than the ones in the S75 set, while the disaggregated fluxes in the S100 set are in all cases less accurate than those in S75 set and with correlation varying depending on the disaggregation method.

When TSEB is used directly with Landsat inputs (Fig. 5d), without performing the disaggregation, a very large negative bias is present reaching the value of -200 W m^{-2}

BGD

11, 4857–4908, 2014

Remotely sensed land-surface energy fluxes

R. Guzinski et al.

Title Page

Abstract

Introduction

Conclusions

References

Tables

Figures

◀

▶

◀

▶

Back

Close

Full Screen / Esc

Printer-friendly Version

Interactive Discussion



for the S75 set (Table 3). This also leads to very high values of RMSE. However, the correlation coefficient is the highest among all the model runs at the GLU site.

4.3.1 Disaggregation when using modeled meteorological inputs

To be able to operationally apply the models at regional scales the tower based meteorological inputs (air temperature, wind speed, relative humidity and incoming short wave radiation) have to be replaced with modeled inputs. As described in Sect. 2.3 the ERA-Interim reanalysis dataset was used in this study. To evaluate the performance of the models when run with the ERA-Interim inputs, the low resolution DTD modeled fluxes, the high resolution fluxes modeled directly with TSEB and Landsat data and the disaggregated high resolution fluxes were compared to measured fluxes at both VOU and GLU flux tower sites. Only the disaggregation algorithm which uses EF as CR is analyzed here since, when tower based meteorological inputs were used, it produced the most accurate results at VOU and reasonably accurate results at GLU.

The results are presented in Fig. 6 and Table 4 for VOU and Fig. 7 and Table 5 for GLU. The first, and surprising, observation is that for all model runs at both VOU and GLU the model accuracy is improved when tower based meteorological observations are replaced by ERA-Interim inputs. This bodes well for performing regional scale modeling using the described methodology. At both sites the disaggregated high resolution fluxes are much more accurate than the directly obtained high resolution fluxes. When S75 set is considered the disaggregation also improves the correlation. When compared to low resolution modeled fluxes the disaggregated fluxes are also more accurate. Especially at VOU when just the S100 set is considered the bias becomes negligible, CV reaches 0.11 and almost perfect correlation is achieved ($R = 0.96$). At GLU the disaggregation reduces the bias and improves the RMSE slightly although the correlation is decreased.

BGD

11, 4857–4908, 2014

Remotely sensed land-surface energy fluxes

R. Guzinski et al.

Title Page

Abstract

Introduction

Conclusions

References

Tables

Figures

◀

▶

◀

▶

Back

Close

Full Screen / Esc

Printer-friendly Version

Interactive Discussion



4.4 Discussion

The results demonstrate that obtaining high resolution fluxes through disaggregation of the low resolution, DTD-derived fluxes is more accurate than obtaining the high resolution fluxes by applying TSEB directly to Landsat data. This implies that there is some extra knowledge in the low resolution flux estimates which is not present in the fluxes derived directly by TSEB. Therefore, it can be inferred that the accuracy of the low resolution estimates is similar to that of the disaggregated fluxes if those estimates were to be compared to flux measurements on the same low resolution spatial scale. By disaggregating the fluxes to a spatial scale below the flux tower footprint we were able to directly compare the modeled and measured fluxes. It should be noted however, that although the Landsat thermal data is provided at 30 m resolution it was acquired at a resolution of between 60 and 120 m depending on the satellite. This could contribute to the uncertainty when comparing the model output with flux tower measurements.

There were substantial differences observed between the two flux tower sites and between the S75 and S100 datasets. In theory, when looking at the non-disaggregated fluxes at both at low and high resolutions (Tables 2–5, columns ND_H and ND_L), the statistical measures of accuracy of the modeled fluxes should be the same for points in the S75 and S100 sets. This is because the membership of the sets was based mostly on the Landsat sensor used: the S100 set had non-stripped observations from Landsat 5 and Landsat 8 while the S75 set contained all the observations, including Landsat 7 observations with a stripe of missing pixels due to sensor failure. In practice, the statistical measures of non-disaggregated modeled fluxes in S75 and S100 sets are only similar at GLU. At VOU the non-disaggregated modeled fluxes in the S75 data set have larger errors and lower correlation than the ones in S100 data set. This could be due to different climatic conditions present at the study sites during the years of operation of the different Landsat satellites. It could also be due to the relatively small number of points present in the data sets not being enough to represent the error distribution.

Remotely sensed land-surface energy fluxes

R. Guzinski et al.

Title Page

Abstract

Introduction

Conclusions

References

Tables

Figures



Back

Close

Full Screen / Esc

Printer-friendly Version

Interactive Discussion



Remotely sensed land-surface energy fluxes

R. Guzinski et al.

Title Page

Abstract

Introduction

Conclusions

References

Tables

Figures



Back

Close

Full Screen / Esc

Printer-friendly Version

Interactive Discussion



At VOU the disaggregated fluxes in the S100 set are much more accurate than those in the S75 set (Tables 2 and 4, columns EF, $LE/R_{s, in}$ and $H/R_{s, in}$). This was expected, since disaggregated fluxes in the S75 set are obtained in less than optimal conditions due to the missing Landsat pixels. Therefore, it can be assumed that if all the pixels were present the relative accuracy of disaggregated fluxes in S75 would be close to the relative accuracy of disaggregated fluxes in S100. By taking this assumption and calculating the ratio of the RMSE of the low resolution and disaggregated fluxes in the S100 set (from Table 4, column EF: $47/19 \approx 2.5$) it can be estimated that if all the Landsat pixels were present the RMSE of all the disaggregated fluxes in the S75 set would be $78/2.5 \approx 30 \text{ W m}^{-2}$. It should also be noted that in all the model runs at VOU, regardless of the pixel size, satellite sensor used or the source of the meteorological inputs, there is one day where the measured sensible heat flux of around 310 W m^{-2} is substantially underestimated (Figs. 3 and 6). Since this underestimation is present in all the model runs, it raises a possibility that the measured flux is inaccurate. If the measurements from this day were removed from the analysis, the accuracy and correlation of the modeled fluxes would be substantially improved.

At GLU the results are different (Tables 3 and 5), with no significant change or even an increase in RMSE and decrease in correlation when low resolution fluxes are disaggregated. The impact of disaggregation was not expected to be as large as at VOU since the landscape at GLU is quite homogeneous at MODIS scale. However the decrease in accuracy was not expected.

There is also a larger difference between the three variations of the disaggregation algorithm at GLU compared to VOU. These differences could be due to large bias in the estimated net radiation at Landsat scale in GLU. The modeled net radiation is consistently underestimated with a bias of around 80 W m^{-2} compared to the tower measurement and around 40 W m^{-2} compared to MODIS scale modeled net radiation (not shown). This could be partly due to the point nature of net radiation measurement vs. the spatially distributed nature of the modeled net radiation or due to inaccurate parametrization of physical parameters, such as LAI or albedo, at Landsat scale at

BGD

11, 4857–4908, 2014

Remotely sensed
land-surface energy
fluxes

R. Guzinski et al.

Title Page

Abstract

Introduction

Conclusions

References

Tables

Figures

◀

▶

◀

▶

Back

Close

Full Screen / Esc

Printer-friendly Version

Interactive Discussion



GLU. For example, at MODIS scale the forested pixels have an albedo of around 0.09 while at Landsat scale that rises to around 0.12–0.15. However, this deficit of available energy must still be distributed among the other fluxes. Depending on which CR method is used the deficit is distributed differently. For example, when $H/R_{s, in}$ is used a larger portion of the available energy is assigned to H to ensure the match with CR on MODIS scale, and this leads to most accurate results when sensible heat fluxes are compared. However, a large portion of the energy deficit will then be assigned to LE leading to its underestimation. A reversal of this situation is encountered when $LE/R_{s, in}$ is used as a constant ratio, which is illustrated by the large bias shown in Table 3. In such situation of net radiation underestimation, using EF as a constant ratio might produce the most balanced results.

Another possible reason why the modeled high resolution fluxes at GLU are less accurate than the low resolution ones is the accuracy of flux tower footprint modeling in the forested landscape. The footprint model assumes a constant roughness and while, as mentioned earlier, the area appears homogeneous at MODIS scale, at Landsat scale different stand ages, roads and clearings become apparent causing the assumption of uniformity to be broken. However, this does not appear to be a major issue as illustrated by the accuracy statistics when TSEB model is used directly with Landsat inputs without disaggregation (Table 3, column ND_H). In this case the correlation between the modeled and observed fluxes is the highest of all the model runs (including the low resolution one) with the correlation coefficient having the value of 0.64 for the S75 set, while the negative bias is at least 6 times as large as in any disaggregated run. The high correlation would indicate that the footprint model, which is the same for all high resolution runs, is working satisfactorily. The bias, on the other hand, once again points to underestimation of net radiation.

Yet another reason for the larger errors over the forested site is the nature of the site and the flux tower setup. For example, due to the large size of the canopy a large amount of heat can be stored in the in-canopy air layer and in the tree biomass (Lindroth et al., 2010). In addition at sites in which the EC equipment is mounted in a tall

BGD

11, 4857–4908, 2014

Remotely sensed
land-surface energy
fluxes

R. Guzinski et al.

Title Page

Abstract

Introduction

Conclusions

References

Tables

Figures



Back

Close

Full Screen / Esc

Printer-friendly Version

Interactive Discussion



tower the 30 min averaging period might not be enough to capture all the contributing eddies (Finnigan et al., 2003). In a previous study Ringgaard et al. (2011) have hypothesized that large scale advection can be a considerable factor in the current study area and at the GLU site in particular. Even though the apparent effects of advection were most significant in winter they might still have impact on the measured fluxes during other periods. It has also been observed that there are significant differences in the fluxes from trees at the edges or inside of the forest stands due to canopy structure (Ringgaard et al., 2012). All those issues affect flux modeling at both high and low spatial resolutions, however they might be less significant at low resolution due to spatial averaging of the modeled fluxes.

Finally, it is worth noting the influence of using model meteorological data (Tables 4 and 5) instead of measured data (Tables 2 and 3). When comparing the RMSE of the S75 dataset in the ND_H (high resolution fluxes derived with TSEB without disaggregation) and ND_L (low resolution fluxes derived with DTD) columns of Table 2 with Table 4 and Table 3 with Table 5 it can be noticed that while there is minimal reduction in error in the TSEB runs, 3 W m⁻² in VOU and 6 W m⁻² in GLU, the reduction in error in the DTD runs is much more significant, 14 W m⁻² in VOU and 23 W m⁻² in GLU. This different behavior of the two models when run with different meteorological data can be caused by the fact that (1) DTD was designed to reduce errors caused by systematic bias in the input temperatures, and (2) that the air temperature estimated by the meteorological forecast and analysis models is representing regional blending height air temperature rather than local, tower measured, air temperature. This indicates that while there is a dominant unsystematic difference between the air temperature measured at the flux tower site and air temperature at another point in the modeling domain, due to different heating of the air from the underlying surfaces, the difference between the modeled blending height temperature at very low resolution (0.75° in case of ERA interim) and air temperature at a point within the modeling domain has a rather dominant systematic bias. This allows DTD to obtain more accurate results with the modeled meteorological inputs, even though from the TSEB performance it appears that the magnitude of the

Remotely sensed land-surface energy fluxes

R. Guzinski et al.

Title Page

Abstract

Introduction

Conclusions

References

Tables

Figures

◀

▶

◀

▶

Back

Close

Full Screen / Esc

Printer-friendly Version

Interactive Discussion



temperature differences between both the measured and modeled air temperatures and air temperature at some point in the modeling domain is similar. The reduction of RMSE in the DTD derived sensible heat flux is propagated through the disaggregation procedure to achieve a reduction of 14 W m^{-2} in RMSE at VOU and 45 W m^{-2} in GLU in case of S100 fluxes disaggregated with EF. This demonstrate the suitability of using modeled meteorological data in conjunction with DTD model to estimate land energy fluxes at regional scales.

5 Conclusions

In the current study we have looked at disaggregating MODIS spatial scale (930 m) sensible heat fluxes derived with the DTD model to Landsat thermal observations' spatial scale (60–120 m resampled to 30 m) using the TSEB model, and the assumption of self preservation of evaporative fraction and ratios of $H/R_{s, \text{in}}$ and $LE/R_{s, \text{in}}$, at a highly heterogeneous agricultural site and a more homogeneous coniferous plantation forest. It was found that using EF as the CR parameter during disaggregation produces the best results at the agricultural site and most balanced results at the forested site. The results at both sites also show that disaggregating the low resolution fluxes to high resolution ones produced more accurate results than when TSEB was applied directly to high resolution Landsat data. This indicates that the low resolution fluxes are accurate at the 1 km spatial scale, since they provide useful additional information to the high resolution fluxes during the disaggregation procedure. It also corroborates the theory raised in the introduction that the discrepancy between fluxes modeled with DTD and measured using tower-based eddy-covariance equipment is in large part due to the scale mismatch between the 930 m model pixel and the measurement footprint, especially at heterogeneous sites.

At the agricultural site the disaggregated high resolution fluxes compare very well with the flux tower measurements with negligible bias, estimated RMSE of 30 W m^{-2} and correlation coefficient very close to 1. At the physically more complex forest site the

disaggregated high resolution fluxes were not so accurate with the low resolution fluxes comparing more favorably to the flux tower measurements. We have also shown that when the tower measured meteorological model inputs are replaced with ERA-Interim model inputs the accuracy of the DTD model, and the disaggregated fluxes, improves which is encouraging for applying the models for the derivation of high resolution fluxes at regional scales. The results show that it is possible to accurately model heat fluxes in highly heterogeneous areas at both MODIS and Landsat spatial scales.

In addition to evaluating the disaggregation procedure we have made a small, but significant, modification to the DTD model by replacing the “parallel” resistance network with “series” resistance network which explicitly takes the in-canopy air temperature into consideration. The modification resulted in large improvement in the accuracy of the modeled fluxes at both the evaluation sites.

Further work should be conducted to better understand the processes occurring in forested ecosystems and to incorporate them into the TSEB models. Additionally, the performance of DTD and the disaggregation procedure when using new generation sensors, such as VIIRS on the Suomi NPP satellite or SLSTR on the upcoming Sentinel-3 satellite, should be evaluated since the Terra and Aqua satellites are already running beyond their expected design life.

Appendix A

A1 TSEB model description

The TSEB model implemented in this study assumes an interaction between the soil and vegetation fluxes, i.e. the flux resistance network is implemented in series (see Fig. 11 in Norman et al., 1995). In the initial state of the model it is assumed that there

BGD

11, 4857–4908, 2014

Remotely sensed land-surface energy fluxes

R. Guzinski et al.

Title Page

Abstract

Introduction

Conclusions

References

Tables

Figures

◀

▶

◀

▶

Back

Close

Full Screen / Esc

Printer-friendly Version

Interactive Discussion



is neutral atmospheric stability, meaning that the Obukhov length, L , is approaching \pm infinity. The actual stability of the boundary layer is later iteratively derived.

Firstly, the parameters which do not depend on L or canopy and soil temperatures, T_C and T_S respectively, are calculated. The fraction of vegetation that is green, $f_g = 1.2 \frac{EVI}{NDVI}$, is estimated for all the land-cover types except for croplands during the growing season (day of year ≤ 180) where it is assumed that the vegetation is fully green (Guzinski et al., 2013). The leaf area index taken from the MCD15A3 MODIS product is assumed to be the green leaf area index, LAI_g . Therefore the total leaf (plant) area index is calculated as $LAI = \frac{LAI_g}{f_g}$ and is used in all the following equations with a symbol F .

The nadir-view clumping factor, Ω_0 , is assigned a value of 1.0 for the croplands and 0.5 for the coniferous forest, although in other studies the clumping factor is estimated (Kustas and Norman, 1999). The fraction of view of the radiometer covered by the vegetation depends on clumping factor and LAI as well as the VZA of the radiometer in radians, θ , and is calculated following Eq. (3) from Norman et al. (2000) as:

$$f(\theta) = 1 - \exp\left(\frac{-0.5\Omega_\theta LAI}{\cos(\theta)}\right) \quad (A1)$$

where Ω_θ is the clumping factor at VZA θ :

$$\Omega_\theta = \frac{\Omega_0}{\Omega_0 + (1 - \Omega_0) \exp(-2.2\theta^{3.8-0.46D})} \quad (A2)$$

D is the ratio of vegetation height to vegetation width which is set to a value of 1.0 for the croplands and 3.5 for the coniferous forest. A maximum limit of 0.95 has to be applied to $f(\theta)$ to ensure that a fraction of soil is always visible to the radiometer. Without this limit T_S calculated by the model can obtain extreme, and hence unrealistic, values.

Equations for deriving displacement height, $d_0 = 0.65h_C$, local roughness length for momentum transport, $z_{OM} = 0.13h_C$, and local roughness length for heat transport,

**Remotely sensed
land-surface energy
fluxes**

R. Guzinski et al.

Title Page

Abstract

Introduction

Conclusions

References

Tables

Figures



Back

Close

Full Screen / Esc

Printer-friendly Version

Interactive Discussion



$Z_{0H} = \frac{z_{0M}}{\exp(2)}$, are taken from Norman et al. (2000) and depend only on vegetation height, h_C .

The net radiation reaching the combined soil and vegetation surface, R_n , is estimated as sum of its shortwave and longwave components, R_s and R_l respectively:

$$R_s = R_{s,in} - R_{s,out} = R_{s,in}(1 - \alpha) \quad (A3)$$

$$R_l = R_{l,in} - R_{l,out} \quad (A4)$$

$$R_{l,in} = \epsilon_{atm} \sigma T_A^4 \quad (A5)$$

$$R_{l,out} = \epsilon_{surf} \sigma T_R^4 - R_{l,in}(1 - \epsilon_{surf}) \quad (A6)$$

where σ is the Stefan Boltzman constant, α is combined soil and vegetation albedo derived from satellite observations, ϵ_{surf} is combined soil and vegetation emissivity also derived from satellite observation and ϵ_{atm} is the emissivity of the atmosphere derived following Brutsaert (1975) as

$$\epsilon_{atm} = 1.24 \left(\frac{ea}{T_A} \right)^{0.14286} \quad (A7)$$

In the above equations air temperature, T_A , and LST, T_R , are in Kelvin.

Once the parameters that remain constant for the duration of an individual TSEB run are calculated, the iterative part of the model can be computed initially with the assumption of $|L| \rightarrow \infty$. First the wind friction velocity, u_* , is calculated following rearranged Eq. (2.54) from Brutsaert (2005):

$$u_* = \frac{uk}{\ln\left(\frac{z_u - d_0}{z_{0M}}\right) - \Psi_M\left(\frac{z_u - d_0}{L}\right) + \Psi_M\left(\frac{z_{0M}}{L}\right)} \quad (A8)$$

where u is the wind speed measured at height z_u , k is the von Karman's constant and $\Psi_M(\zeta)$ is Monin–Obukhov stability correction function for momentum calculated as in

**Remotely sensed
land-surface energy
fluxes**

R. Guzinski et al.

Title Page

Abstract

Introduction

Conclusions

References

Tables

Figures

◀

▶

◀

▶

Back

Close

Full Screen / Esc

Printer-friendly Version

Interactive Discussion



Eqs. (2.59) and (2.63) of Brutsaert (2005):

$$\Psi_M(\zeta) = -6.1 \ln[\zeta + (1 + \zeta^{2.5})^{\frac{1}{2.5}}], \quad \zeta \geq 0 \quad (\text{A9})$$

$$\Psi_M(y) = \ln(a + y) - 3by^{\frac{1}{3}} + \frac{ba^{\frac{1}{3}}}{2} \ln \left[\frac{(1+x)^2}{1-x+x^2} \right] + 3^{\frac{1}{2}} ba^{\frac{1}{3}} \tan^{-1} \left[\frac{2x-1}{3^{\frac{1}{2}}} \right] + \Psi_0, \quad \zeta < 0 \quad (\text{A10})$$

- 5 where $\zeta = \frac{z_u - d_0}{L}$ or $\zeta = \frac{z_{0M}}{L}$ as required, $y = -\zeta$, $x = (\frac{y}{a})^{\frac{1}{3}}$, $\Psi_0 = -\ln(a) + 3^{\frac{1}{2}} ba^{\frac{1}{3}} \frac{\pi}{6}$, $a = 0.33$ and $b = 0.41$. In the second equation the value of y is limited such that $y \leq b^{-3}$. In neutral atmospheric stability condition, when $|L| \rightarrow \infty$, the stability correction function is 0.

There are three resistances in the soil–canopy–atmosphere heat flux network: R_A – aerodynamic resistance to heat transport in the surface layer, R_S – resistance to heat transport from the soil surface and R_x – the total boundary layer resistance of the leaf canopy. The first resistance is estimated following Norman et al. (2000) as:

$$R_A = \frac{\ln(\frac{z_T - d_0}{z_{0H}}) - \Psi_H(\frac{z_T - d_0}{L}) + \Psi_H(\frac{z_{0H}}{L})}{u_* k} \quad (\text{A11})$$

15 where $\Psi_H(\zeta)$ is the Monin–Obukhov stability function for heat, calculated in the same way as $\Psi_M(\zeta)$ for stable conditions and as in Eq. (2.64) from Brutsaert (2005) for unstable conditions:

$$\Psi_H(y) = \frac{1-d}{n} \ln \left(\frac{c+y^n}{c} \right), \quad \zeta < 0 \quad (\text{A12})$$

20 where $y = -\zeta$, $c = 0.33$, $d = 0.057$ and $n = 0.78$.

Calculation of R_S is also taken from Norman et al. (2000):

$$R_S = \frac{1}{c_T + bu_S} \quad (\text{A13})$$

Title Page

Abstract

Introduction

Conclusions

References

Tables

Figures

◀

▶

◀

▶

Back

Close

Full Screen / Esc

Printer-friendly Version

Interactive Discussion



In the above equation the parameter c_T is varying smoothly from value of 0.006 for LAI less than 2 to 0.004 for LAI more than 2, b is a constant with value of 0.012 and u_S is the wind speed just above the soil surface and is determined from wind speed just above the canopy, u_C , as follows (Norman et al., 1995):

$$u_C = \ln \left(\frac{h_C - d_0}{z_{0M}} \right) \frac{u_*}{k} \quad (\text{A14})$$

$$u_S = u_C \exp \left(-a \left(1 - \frac{h_S}{h_C} \right) \right) \quad (\text{A15})$$

$$a = 0.28(F\Omega_0)^{\frac{2}{3}} h_C^{\frac{1}{3}} s^{-\frac{1}{3}} \quad (\text{A16})$$

where s is the leaf size in meters, h_S is set to 0.05 m and h_C has a minimum limit of 0.5 m in the u_S equation. The final resistance R_x is calculated as (Norman et al., 1995):

$$R_x = \frac{C'}{F} \left(\frac{s}{u_d} \right)^{0.5} \quad (\text{A17})$$

where C' is a constant with value of 90 and u_d is wind speed at height $d_0 + z_{0M}$ and is derived using the equation for u_S with $h_S = d_0 + z_{0M}$.

Once the values of the three resistances are known the temperature of the canopy, T_C , soil, T_S , and the inter-canopy air, T_{AC} can be estimated. Firstly, the energy divergence in the canopy, ΔR_n , has to be established. During the first iteration, when T_C and T_S are not yet known, the shortwave and longwave components of the net radiation are lumped together, following Eq. (5b) from (Norman et al., 2000):

$$\Delta R_n = R_n \left[1 - \exp \left(\frac{-\kappa F \Omega_0}{2 \cos(\theta_s)^{0.5}} \right) \right] \quad (\text{A18})$$

where θ_s is the sun zenith angle and κ is a parameter varying smoothly from 0.45 for LAI more than 2 to 0.8 for LAI less than 2. In the following iterations the divergence of

BGD

11, 4857–4908, 2014

Remotely sensed land-surface energy fluxes

R. Guzinski et al.

Title Page

Abstract

Introduction

Conclusions

References

Tables

Figures

◀

▶

◀

▶

Back

Close

Full Screen / Esc

Printer-friendly Version

Interactive Discussion



shortwave and longwave radiation is treated explicitly so that $\Delta R_n = \Delta R_s + \Delta R_l$. ΔR_s is calculated the same as ΔR_n in the first iteration with R_n replaced by R_s while ΔR_l is calculated as in Eq. (2b) of Kustas and Norman (1999):

$$\Delta R_l = \tau(R_{l,sky} + R_{l,S} - 2R_{l,C}) \quad (A19)$$

where $R_{l,sky}$ is the longwave radiation from the sky calculated as in Eq. (A5) and $R_{l,S}$ and $R_{l,C}$ are longwave radiation emitted from soil and canopy respectively and calculated using Stefan–Boltzman equation and T_S and T_C . τ is the transmissivity of the vegetation estimated as $\tau = 1 - \exp(\kappa_L F)$ and κ_L varies smoothly between 0.7 for LAI more than 1 and 0.95 for LAI less than 1. With ΔR_n it is possible to estimate the sensible heat flux of the canopy by using the Priestly–Taylor approximation (Norman et al., 2000):

$$H_C = \Delta R_n \left(1 - \alpha_{PT} f_g \frac{sp}{sp + \gamma} \right) \quad (A20)$$

Initially it is assumed that the vegetation is transpiring at potential rate and the Priestly–Taylor parameter, α_{PT} , has a value of 1.26. If implausible results are obtained, α_{PT} can be reduced as explained later. sp is the slope of the saturation pressure curve and γ is the psychometric constant and both were obtained from Annex 3 of Allen et al. (1998). With the value of H_C the temperature of the canopy can be estimated following (Norman et al., 1995) as:

$$T_C = T_{C,lin} + \Delta T_C \quad (A21)$$

where $T_{C,lin}$ is the linear approximation of the canopy temperature:

$$T_{C,lin} = \frac{\frac{T_A}{R_A} + \frac{T_R}{R_S(1-f_\theta)} + \frac{H_C R_x}{\rho c_p} \left(\frac{1}{R_A} + \frac{1}{R_S} + \frac{1}{R_x} \right)}{\frac{1}{R_A} + \frac{1}{R_S} + \frac{f_\theta}{R_S(1-f_\theta)}} \quad (A22)$$

and ΔT_C is the correction factor:

$$\Delta T_C = \frac{T_R^4 - f_\theta T_{C,\text{lin}}^4 - (1 - f_\theta) T_D^4}{4(1 - f_\theta) T_D^3 \left(1 + \frac{R_S}{R_A}\right) + 4f_\theta T_{C,\text{lin}}^3} \quad (\text{A23})$$

where

$$T_D = T_{C,\text{lin}} \left(1 + \frac{R_S}{R_A}\right) - \frac{H_C R_x}{\rho c_p} \left(1 + \frac{R_S}{R_x} + \frac{R_S}{R_A}\right) - T_A \frac{R_S}{R_A} \quad (\text{A24})$$

The soil temperature can now be estimated from the canopy temperature, the T_R and the viewing geometry:

$$T_S = \left(\frac{T_R^4 - f_\theta T_C^4}{1 - f_\theta}\right)^{0.25} \quad (\text{A25})$$

Finally the inter-canopy air temperature can be estimated:

$$T_{AC} = \frac{\frac{T_A}{R_A} + \frac{T_S}{R_S} + \frac{T_C}{R_x}}{\frac{1}{R_A} + \frac{1}{R_S} + \frac{1}{R_x}} \quad (\text{A26})$$

With all the resistances and component temperatures now known it is finally possible to calculate the fluxes. Firstly, the canopy fluxes are calculated:

$$H_C = \rho c_p \frac{T_C - T_{AC}}{R_x} \quad (\text{A27})$$

$$LE_C = \Delta R_n - H_C \quad (\text{A28})$$

Those are followed by soil fluxes:

$$H_S = \rho c_p \frac{T_S - T_{AC}}{R_S} \quad (\text{A29})$$

Title Page

Abstract

Introduction

Conclusions

References

Tables

Figures

◀

▶

◀

▶

Back

Close

Full Screen / Esc

Printer-friendly Version

Interactive Discussion



$$R_{n,S} = R_n - \Delta R_n \quad (\text{A30})$$

$$G = -0.3R_{n,S} - 35 \quad (\text{A31})$$

$$LE_S = R_{n,S} - G - H_S \quad (\text{A32})$$

5 where G represents the soil heat flux and the equation is based on Liebethal and Foken (2007). The total sensible and latent heat fluxes are taken as the sum of their canopy and soil components:

$$H = H_C + H_S = \rho c_p \frac{T_{AC} - T_A}{R_A} \quad (\text{A33})$$

$$10 \quad LE = LE_C + LE_S \quad (\text{A34})$$

With the values of H and LE it is possible to recalculate L using the Eq. (2.46) from Brutsaert (2005):

$$L = - \frac{u_*^3}{\frac{kg}{T_A} \left(\frac{H}{\rho c_p} + 0.61 T_A \frac{E}{\rho} \right)} \quad (\text{A35})$$

15 where g is gravitational constant with value of 9.8 and E is the rate of surface evaporation in $\text{kgm}^{-2}\text{s}^{-1}$ derived from LE using the equation from Annex 3 of Allen et al. (1998). The iterative part of the model is now re-run with the new value of L and the process is repeated until L converges to a stable value.

20 Once L stabilizes, if the value of LE_S is negative it means that the canopy transpiration has been overestimated and α_{PT} has to be reduced and the iterative part of the model repeated once again. If α_{PT} reaches zero and the modeled LE_S is still negative then it is considered that there is no evaporation or transpiration in the modeled pixel (Norman et al., 1995). In those cases $LE = LE_S = LE_C = 0$ and since $\alpha_{PT} = 0$ it follows from Eq. (A20) that $H_C = \Delta R_n$. H can then be estimated as normally and the output value limited such that $H \leq R_n - G$. The limit is enforced since it is implausible that on
25 a dry day without evapotranspiration the ground heat flux would be negative or nil. If $H < R_n - G$ then any residual energy is assigned to G .

**Remotely sensed
land-surface energy
fluxes**

R. Guzinski et al.

Title Page	
Abstract	Introduction
Conclusions	References
Tables	Figures
◀	▶
◀	▶
Back	Close
Full Screen / Esc	
Printer-friendly Version	
Interactive Discussion	



A2 DTD model description

The DTD model replaces the observations of absolute air temperature and LST with their time-differential values, taken as a difference between a night-time observation and another one in the late morning or early afternoon (Guzinski et al., 2013). Therefore, although it uses many of the TSEB model formulations, some of the key equations have been modified. In the original DTD formulation one of the changes is the replacement of the “series” flux resistance network by a “parallel” one (see Fig. 1 in Norman et al., 1995). The later one is a simpler formulation which ignores the interaction between soil and vegetation fluxes and potentially can produce less accurate results (Kustas and Norman, 1999).

The main DTD equation is derived by applying Eq. (14) from Anderson et al. (1997) to night-time and day-time temperature observations, taking the difference of the two and simplifying by removing insignificant early morning, or night-time, fluxes (Norman et al., 2000):

$$H_1 = \rho c_p \left[\frac{(T_{R,1}(\theta_1) - T_{R,0}(\theta_0)) - (T_{A,1} - T_{A,0})}{(1 - f(\theta_1))(R_{A,1} + R_{S,1})} \right] + H_{C,1} \left[1 - \frac{f(\theta_1)}{1 - f(\theta_1)} \frac{R_{A,1}}{R_{A,1} + R_{S,1}} \right] \quad (\text{A36})$$

The subscripts 0 and 1 in the above equation, and in all the following equations, refer to observations taken at night and during the day respectively. $f(\theta_1)$ can be calculated in the same fashion as in the TSEB model. The sensible heat flux of the canopy, $H_{C,1}$, is derived using Eq. (A20) from the TSEB model with ΔR_n estimated with the shortwave and longwave components of R_n lumped together. The resistances used in the “parallel” resistance network, R_A and R_S , can be also calculated using the same equations as in TSEB. However, there is one important change in that the Richardson number, Ri, is used as an approximation for $\frac{z_u - d_0}{L}$ in all the resistance equations. Ri is calculated using time-differential observations as in Norman et al. (2000):

$$\text{Ri} = -g \frac{z_u - d_0}{T_{A1}} \frac{(T_{R1} - T_{R0}) - (T_{A1} - T_{A0})}{u_1^2} \quad (\text{A37})$$

In this study a formulation for estimating H_1 in the DTD model using the “series” resistance network has been developed. It follows the principles used in deriving Eq. (A36), by first taking a linear approximation of Eq. (1) and combining it with Eqs. (A27), (A29) and (A33) to obtain:

$$T_R - T_A = \frac{H[(1 - f(\theta))R_S + R_A]}{\rho c_p} + \frac{H_C[f(\theta)R_x - (1 - f(\theta))R_S]}{\rho c_p} \quad (\text{A38})$$

The above equation is then applied at two times, subscripted with 0 and 1, and rearranged to derive:

$$H_1 = \rho c_p \frac{(T_{R,1}(\theta_1) - T_{R,0}(\theta_0)) - (T_{A,1} - T_{A,0})}{(1 - f(\theta_1))R_{S,1} + R_{A,1}} + \frac{H_{C,1}[(1 - f(\theta_1))R_{S,1} - f(\theta_1)R_{x,1}]}{(1 - f(\theta_1))R_{S,1} + R_{A,1}} + \frac{H_0[(1 - f(\theta_0))R_{S,0} + R_{A,0}]}{(1 - f(\theta_1))R_{S,1} + R_{A,1}} + \frac{H_{C,0}[f(\theta_0)R_{x,0} - (1 - f(\theta_0))R_{S,0}]}{(1 - f(\theta_1))R_{S,1} + R_{A,1}} \quad (\text{A39})$$

Since the first time, with subscript 0, is chosen when fluxes are minimal the last two terms of the above equation can be omitted similarly to what is done in the original DTD model.

The latent heat flux is calculated as residual of the other fluxes:

$$LE_1 = R_{n,1} - H_1 - G_1 \quad (\text{A40})$$

The estimation of G_1 is changed from that in the TSEB model since $T_{R,1} - T_{R,0}$ can be used as approximation of the diurnal variation in the soil surface temperature, ΔT_R , and this allows the usage of a more advanced soil heat flux model from Santanello and Friedl (2003):

$$G = R_{n,S} A \cos\left(2\pi \frac{t + 10800}{B}\right) \quad (\text{A41})$$

$$A = 0.0074\Delta T_R + 0.088 \quad (\text{A42})$$

$$B = 1729\Delta T_R + 65013 \quad (\text{A43})$$

t is the time in seconds between the observation time and the solar noon and $R_{n,S}$ is the net radiation reaching the soil if the sun is in nadir calculated as $R_{n,S} = R_n \exp(\kappa F \Omega_0)$ where κ varies smoothly between 0.45 for LAI more than 2 to 0.8 for LAI less than 2 and Ω_0 is the nadir view clumping factor.

Once all of the above fluxes are estimated the latent heat flux of the soil can be also derived as residual:

$$\text{LE}_{S,1} = (R_{n,1} - \Delta R_{n,1}) - (H_1 - H_{C,1}) - G_1 \quad (\text{A44})$$

Similarly to TSEB is $\text{LE}_{S,1}$ is negative it is considered that the canopy transpiration has been overestimated and therefore α_{PT} is reduced and $H_{C,1}$, H_1 and $\text{LE}_{S,1}$ are recalculated. If $\text{LE}_{S,1}$ is still negative when α_{PT} reaches a value of zero the same procedure is followed as in the TSEB model.

Acknowledgements. The work has been carried out under the HOBE project funded by the VILLUM FOUNDATION. We would like to thank the people maintaining the HOBE flux towers (Lars Rasmussen, Anton Thomsen).



This publication is supported
by COST – www.cost.eu

References

- Allen, R. G., Pereira, L. S., Raes, D., and Smith, M.: Crop evapotranspiration – Guidelines for computing crop water requirements – FAO Irrigation and drainage paper 56, FAO, Rome, 300, 6541, 1998. 4886, 4888
- Anderson, G. P., Felde, G. W., Hoke, M. L., Ratkowski, A. J., Cooley, T. W., Chetwynd Jr., J. H., Gardner, J., Adler-Golden, S. M., Matthew, M. W., Berk, A. et al.: MODTRAN4-based atmospheric correction algorithm: FLAASH (Fast Line-of-sight Atmospheric Analysis of Spectral

Remotely sensed land-surface energy fluxes

R. Guzinski et al.

Title Page

Abstract

Introduction

Conclusions

References

Tables

Figures



Back

Close

Full Screen / Esc

Printer-friendly Version

Interactive Discussion



BGD

11, 4857–4908, 2014

Remotely sensed
land-surface energy
fluxes

R. Guzinski et al.

Title Page

Abstract

Introduction

Conclusions

References

Tables

Figures

◀

▶

◀

▶

Back

Close

Full Screen / Esc

Printer-friendly Version

Interactive Discussion



Hypercubes), in: AeroSense 2002, International Society for Optics and Photonics, 65–71, 2002. 4865

Anderson, M., Norman, J., Diak, G., Kustas, W., and Mecikalski, J.: A two-source time-integrated model for estimating surface fluxes using thermal infrared remote sensing, *Remote Sens. Environ.*, 60, 195–216, 1997. 4859, 4860, 4867, 4868, 4889

Anderson, M. C., Norman, J., Mecikalski, J. R., Torn, R. D., Kustas, W. P., and Basara, J. B.: A multiscale remote sensing model for disaggregating regional fluxes to micrometeorological scales, *J. Hydrometeorol.*, 5, 343–363, 2004. 4860, 4861, 4868

Anderson, M. C., Kustas, W. P., Norman, J. M., Hain, C. R., Mecikalski, J. R., Schultz, L., González-Dugo, M. P., Cammalleri, C., d'Urso, G., Pimstein, A., and Gao, F.: Mapping daily evapotranspiration at field to continental scales using geostationary and polar orbiting satellite imagery, *Hydrol. Earth Syst. Sci.*, 15, 223–239, doi:10.5194/hess-15-223-2011, 2011. 4860

Bastiaanssen, W., Menenti, M., Feddes, R., and Holtslag, A.: A remote sensing surface energy balance algorithm for land (SEBAL), 1. Formulation, *J. Hydrol.*, 212, 198–212, 1998. 4859

Berk, A., Anderson, G. P., Acharya, P. K., Bernstein, L. S., Muratov, L., Lee, J., Fox, M., Adler-Golden, S. M., Chetwynd Jr., J. H., Hoke, L. et al.: MODTRAN5: 2006 update, in: *Proc. SPIE*, vol. 6233, 8 pp., 2006. 4864

Brutsaert, W.: On a derivable formula for long-wave radiation from clear skies, *Water Resour. Res.*, 11, 742–744, 1975. 4883

Brutsaert, W.: *Hydrology, An Introduction*, Cambridge University Press, 2005. 4883, 4884, 4888

Burba, G. G., McDermitt, D. K., Grelle, A., Anderson, D. J., and Xu, L.: Addressing the influence of instrument surface heat exchange on the measurements of CO₂ flux from open-path gas analyzers, *Glob. Change Biol.*, 14, 1854–1876, 2008. 4863

Cammalleri, C., Anderson, M. C., Gao, F., Hain, C. R., and Kustas, W. P.: A data fusion approach for mapping daily evapotranspiration at field scale, *Water Resour. Res.*, 49, 4672–4686, doi:10.1002/wrcr.20349, 2013a. 4869

Cammalleri, C., Anderson, M. C., and Kustas, W. P.: Upscaling of evapotranspiration fluxes from instantaneous to daytime scales for thermal remote sensing applications, *Hydrol. Earth Syst. Sci. Discuss.*, 10, 7325–7350, doi:10.5194/hessd-10-7325-2013, 2013b. 4869

Coll, C., Galve, J. M., Sanchez, J. M., and Caselles, V.: Validation of Landsat-7/ETM+ thermal-band calibration and atmospheric correction with ground-based measurements, *IEEE T. Geosci. Remote*, 48, 547–555, 2010. 4865

Remotely sensed land-surface energy fluxes

R. Guzinski et al.

Title Page

Abstract

Introduction

Conclusions

References

Tables

Figures

◀

▶

◀

▶

Back

Close

Full Screen / Esc

Printer-friendly Version

Interactive Discussion



Dee, D., Uppala, S., Simmons, A., Berrisford, P., Poli, P., Kobayashi, S., Andrae, U., Bal-
maseda, M., Balsamo, G., Bauer, P. et al.: The ERA-Interim reanalysis: configuration and
performance of the data assimilation system, *Q. J. Roy. Meteor. Soc.*, 137, 553–597, 2011.
4865

Detto, M., Montaldo, N., Albertson, J. D., Mancini, M., and Katul, G.: Soil moisture and vege-
tation controls on evapotranspiration in a heterogeneous Mediterranean ecosystem on Sar-
dinia, Italy, *Water Resour. Res.*, 42, 8, doi:10.1029/2005WR004693, 2006. 4870

Finnigan, J., Clement, R., Malhi, Y., Leuning, R., and Cleugh, H.: A re-evaluation of long-term
flux measurement techniques part I: averaging and coordinate rotation, *Bound.-Lay. Meteorol.*, 107, 1–48, 2003. 4864, 4879

Foken, T., Aubinet, M., Finnigan, J. J., Leclerc, M. Y., Mauder, M., and Paw U., and Kyaw, T.:
Results of a panel discussion about the energy balance closure correction for trace gases,
B. Am. Meteorol. Soc., 92, 13–18, 2011. 4864

Gao, F., Anderson, M. C., Kustas, W. P., and Wang, Y.: Simple method for retrieving leaf area
index from Landsat using MODIS leaf area index products as reference, *J. Appl. Remote
Sens.*, 6, 1–15, 2012. 4865

Guzinski, R., Anderson, M. C., Kustas, W. P., Nieto, H., and Sandholt, I.: Using a thermal-
based two source energy balance model with time-differencing to estimate surface en-
ergy fluxes with day–night MODIS observations, *Hydrol. Earth Syst. Sci.*, 17, 2809–2825,
doi:10.5194/hess-17-2809-2013, 2013. 4860, 4861, 4864, 4867, 4882, 4889

Hsieh, C.-I., Katul, G., and Chi, T.-W.: An approximate analytical model for footprint estimation
of scalar fluxes in thermally stratified atmospheric flows, *Adv. Water Resour.*, 23, 765–772,
2000. 4871

Knyazikhi, Y., Glassy, J., Privette, J. L., Tian, Y., Lotsch, A., Zhang, Y., Wang, Y., Morissette, J. T.,
Votava, P., Myneni, R., Nemani, R. R., and Running, S. W.: MODIS Leaf Area Index (LAI)
and Fraction of Photosynthetically Active Radiation Absorbed by Vegetation (FPAR) Product
(MOD15) Algorithm Theoretical Basis Document, available at: <http://eosps0.gsfc.nasa.gov/atbd/modistables.html>, 1999. 4864

Kustas, W., Li, F., Jackson, T., Prueger, J., MacPherson, J., and Wolde, M.: Effects of remote
sensing pixel resolution on modeled energy flux variability of croplands in Iowa, *Remote
Sens. Environ.*, 92, 535–547, 2004. 4859

Remotely sensed land-surface energy fluxes

R. Guzinski et al.

[Title Page](#)

[Abstract](#)

[Introduction](#)

[Conclusions](#)

[References](#)

[Tables](#)

[Figures](#)

[⏪](#)

[⏩](#)

[◀](#)

[▶](#)

[Back](#)

[Close](#)

[Full Screen / Esc](#)

[Printer-friendly Version](#)

[Interactive Discussion](#)

- Kustas, W. P. and Albertson, J. D.: Effects of surface temperature contrast on land-atmosphere exchange: a case study from Monsoon 90, *Water Resour. Res.*, 39, 6, doi:10.1029/2001WR001226, 2003. 4859, 4868
- Kustas, W. P. and Norman, J. M.: Evaluation of soil and vegetation heat flux predictions using a simple two-source model with radiometric temperatures for partial canopy cover, *Agr. Forest Meteorol.*, 94, 13–29, 1999. 4866, 4882, 4886, 4889
- Kustas, W. P., Alfieri, J. G., Anderson, M. C., Colaizzi, P. D., Prueger, J. H., Evett, S. R., Neale, C. M., French, A. N., Hipps, L. E., Chávez, J. L. et al.: Evaluating the two-source energy balance model using local thermal and surface flux observations in a strongly advective irrigated agricultural area, *Adv. Water Resour.*, 50, 120–133, 2012. 4864
- Li, F., Jackson, T. J., Kustas, W. P., Schmugge, T. J., French, A. N., Cosh, M. H., and Bindlish, R.: Deriving land surface temperature from Landsat 5 and 7 during SMEX02/SMACEX, *Remote Sens. Environ.*, 92, 521–534, 2004. 4859
- Liebenthal, C. and Foken, T.: Evaluation of six parameterization approaches for the ground heat flux, *Theor. Appl. Climatol.*, 88, 43–56, doi:10.1007/s00704-005-0234-0, 2007. 4888
- Lindroth, A., Mölder, M., and Lagergren, F.: Heat storage in forest biomass improves energy balance closure, *Biogeosciences*, 7, 301–313, doi:10.5194/bg-7-301-2010, 2010. 4878
- Mauder, M. and Foken, T.: Impact of post-field data processing on eddy covariance flux estimates and energy balance closure, *Meteorol. Z.*, 15, 597–609, 2006. 4863
- Moncrieff, J. B., Massheder, J., De Bruin, H., Elbers, J., Friborg, T., Heusinkveld, B., Kabat, P., Scott, S., Søgaard, H., and Verhoef, A.: A system to measure surface fluxes of momentum, sensible heat, water vapour and carbon dioxide, *J. Hydrol.*, 188, 589–611, 1997. 4863
- Norman, J., Kustas, W., and Humes, K.: A two-source approach for estimating soil and vegetation fluxes from observations of directional radiometric surface temperature, *Agr. Forest Meteorol.*, 77, 263–293, doi:10.1016/0168-1923(95)02265-Y, 1995. 4859, 4866, 4868, 4871, 4881, 4885, 4886, 4888, 4889
- Norman, J., Anderson, M., Kustas, W., French, A., Mecikalski, J., Torn, R., Diak, G., Schmugge, T., and Tanner, B.: Remote sensing of surface energy fluxes at 101-m pixel resolutions, *Water Resour. Res.*, 39, 8, doi:10.1029/2002WR001775, 2003. 4861, 4868
- Norman, J. M., Kustas, W. P., Prueger, J. H., and Diak, G. R.: Surface flux estimation using radiometric temperature: a dual-temperature-difference method to minimize measurement errors, *Water Resour. Res.*, 36, 2263, doi:10.1029/2000WR900033, 2000. 4860, 4867, 4882, 4883, 4884, 4885, 4886, 4889

Remotely sensed land-surface energy fluxes

R. Guzinski et al.

Title Page

Abstract

Introduction

Conclusions

References

Tables

Figures

◀

▶

◀

▶

Back

Close

Full Screen / Esc

Printer-friendly Version

Interactive Discussion



- Papale, D., Reichstein, M., Aubinet, M., Canfora, E., Bernhofer, C., Kutsch, W., Longdoz, B., Rambal, S., Valentini, R., Vesala, T., and Yakir, D.: Towards a standardized processing of Net Ecosystem Exchange measured with eddy covariance technique: algorithms and uncertainty estimation, *Biogeosciences*, 3, 571–583, doi:10.5194/bg-3-571-2006, 2006. 4863
- 5 Peng, J., Borsche, M., Liu, Y., and Loew, A.: How representative are instantaneous evaporative fraction measurements of daytime fluxes?, *Hydrol. Earth Syst. Sci.*, 17, 3913–3919, doi:10.5194/hess-17-3913-2013, 2013. 4869
- Priestley, C. H. B. and Taylor, R. J.: On the assessment of surface heat flux and evaporation using large-scale parameters, *Mon. Weather Rev.*, 100, 81–92, doi:10.1175/1520-0493(1972)100<0081:OTAOSH>2.3.CO;2, 1972. 4867
- 10 Reichstein, M., Falge, E., Baldocchi, D., Papale, D., Aubinet, M., Berbigier, P., Bernhofer, C., Buchmann, N., Gilmanov, T., Granier, A., Grünwald, T., Havránková, K., Ilvesniemi, H., Janous, D., Knohl, A., Laurila, T., Lohila, A., Loustau, D., Matteucci, G., Meyers, T., Miglietta, F., Ourcival, J.-M., Pumpanen, J., Rambal, S., Rotenberg, E., Sanz, M., Tenhunen, J., Seufert, G., Vaccari, F., Vesala, T., Yakir, D., and Valentini, R.: On the separation of net ecosystem exchange into assimilation and ecosystem respiration: review and improved algorithm, *Glob. Change Biol.*, 11, 1424–1439, doi:10.1111/j.1365-2486.2005.001002.x, 2005. 4863
- 15 Ringgaard, R., Herbst, M., Friborg, T., Schelde, K., Thomsen, A. G., and Soegaard, H.: Energy fluxes above three disparate surfaces in a temperate mesoscale coastal catchment, *Vadose Zone J.*, 10, 54–66, doi:10.2136/vzj2009.0181, 2011. 4863, 4879
- Ringgaard, R., Herbst, M., and Friborg, T.: Partitioning of forest evapotranspiration: the impact of edge effects and canopy structure, *Agr. Forest Meteorol.*, 166, 86–97, 2012. 4862, 4879
- Santanello, J. A. and Friedl, M. A.: Diurnal covariation in soil heat flux and net radiation, *J. Appl. Meteorol.*, 42, 851–862, 2003. 4890
- 25 Schmid, H.: Source areas for scalars and scalar fluxes, *Bound.-Lay. Meteorol.*, 67, 293–318, 1994. 4871
- Sobrino, J. A., Jiménez-Muñoz, J. C., and Paolini, L.: Land surface temperature retrieval from LANDSAT TM 5, *Remote Sens. Environ.*, 90, 434–440, 2004. 4859
- 30 Stisen, S., Sandholt, I., Nørgaard, A., Fensholt, R., and Eklundh, L.: Estimation of diurnal air temperature using MSG SEVIRI data in West Africa, *Remote Sens. Environ.*, 110, 262–274, 2007. 4865

Remotely sensed land-surface energy fluxes

R. Guzinski et al.

Title Page

Abstract

Introduction

Conclusions

References

Tables

Figures



Back

Close

Full Screen / Esc

Printer-friendly Version

Interactive Discussion



Stisen, S., Sandholt, I., Nørgaard, A., Fensholt, R., and Jensen, K. H.: Combining the triangle method with thermal inertia to estimate regional evapotranspiration – applied to MSG-SEVIRI data in the Senegal River basin, *Remote Sens. Environ.*, 112, 1242–1255, 2008. 4859

Verhoef, W. and Bach, H.: Simulation of hyperspectral and directional radiance images using coupled biophysical and atmospheric radiative transfer models, *Remote Sens. Environ.*, 87, 23–41, 2003. 4865

Wan, Z.: MODIS Land Surface Temperature Products Users' Guide, available at: <http://www.icesc.ucsb.edu/modis/LstUsrGuide/usrguide.html> (accessed 14 February 2012), 2006. 4864

Webb, E. K., Pearman, G. I., and Leuning, R.: Correction of flux measurements for density effects due to heat and water vapour transfer, *Q. J. Roy. Meteor. Soc.*, 106, 85–100, 1980. 4863

Wilczak, J. M., Oncley, S. P., and Stage, S. A.: Sonic anemometer tilt correction algorithms, *Bound.-Lay. Meteorol.*, 99, 127–150, 2001. 4863

Xu, Y., Wang, R., Liu, S., Yang, S., and Yan, B.: Atmospheric correction of hyperspectral data using MODTRAN model, in: *Remote Sensing of the Environment: 16th National Symposium on Remote Sensing of China*, 712306–712306, International Society for Optics and Photonics, 2008. 4865

Zhu, Z. and Woodcock, C. E.: Object-based cloud and cloud shadow detection in Landsat imagery, *Remote Sens. Environ.*, 118, 83–94, 2012. 4865

Remotely sensed
land-surface energy
fluxes

R. Guzinski et al.

Title Page

Abstract

Introduction

Conclusions

References

Tables

Figures

◀

▶

◀

▶

Back

Close

Full Screen / Esc

Printer-friendly Version

Interactive Discussion



Table 1. Statistical comparison of modeled vs. measured sensible and latent heat fluxes at VOU and GLU for the “parallel” and “series” implementation of DTD. The statistical parameters used are bias (modeled–measured), root mean square error (RMSE), coefficient of variation (CV – RMSE divided by mean of observed values), and correlation (r). Bias and RMSE are in Wm^{-2} , the other parameters are unitless.

Site	Implementation	H				LE			
		Bias	RMSE	CV	r	Bias	RMSE	CV	r
VOU	parallel	124	184	1.42	0.19	–114	167	0.54	0.23
	series	35	107	0.81	0.20	–30	107	0.35	0.42
GLU	parallel	134	183	0.60	0.64	–187	226	0.80	0.07
	series	65	135	0.45	0.59	–122	173	0.62	0.19

Remotely sensed land-surface energy fluxes

R. Guzinski et al.

Table 2. Statistical comparison of modeled vs. measured sensible heat flux at VOU for the three approaches used to estimate the constant ratio used during the disaggregation procedure and for the non-disaggregated high, ND_H , and low, ND_L , resolution fluxes. The statistical parameters used are bias (modeled–measured), root mean square error (RMSE), coefficient of variation (CV – RMSE divided by mean of observed values), and correlation (r). Bias and RMSE are in Wm^{-2} , the other parameters are unitless.

		EF	$LE/R_{s, in}$	$H/R_{s, in}$	ND_H	ND_L
Bias	S75	–2	–12	6	–32	23
	S100	–14	–23	–5	–7	26
RMSE	S75	68	71	75	79	92
	S100	32	39	37	66	72
CV	S75	0.45	0.47	0.50	0.50	0.59
	S100	0.20	0.25	0.23	0.42	0.46
r	S75	0.65	0.63	0.63	0.71	0.41
	S100	0.94	0.92	0.93	0.84	0.69

Title Page

Abstract

Introduction

Conclusions

References

Tables

Figures

◀

▶

◀

▶

Back

Close

Full Screen / Esc

Printer-friendly Version

Interactive Discussion



Remotely sensed land-surface energy fluxes

R. Guzinski et al.

Table 3. Statistical comparison of modeled vs. measured sensible heat flux at GLU for the three approaches used to estimate the constant ratio used during the disaggregation procedure and for the non-disaggregated high, ND_H , and low, ND_L , resolution fluxes. The statistical parameters used are bias (modeled–measured), root mean square error (RMSE), coefficient of variation (CV – RMSE divided by mean of observed values), and correlation (r). Bias and RMSE are in Wm^{-2} , the other parameters are unitless.

		EF	$LE/R_{s, in}$	$H/R_{s, in}$	ND_H	ND_L
Bias	S75	–11	–30	–12	–200	45
	S100	–32	–53	–19	–193	23
RMSE	S75	119	131	107	218	125
	S100	134	149	136	210	131
CV	S75	0.37	0.41	0.33	0.67	0.37
	S100	0.38	0.43	0.40	0.62	0.38
r	S75	0.38	0.33	0.49	0.64	0.40
	S100	0.37	0.37	0.28	0.65	0.41

Title Page

Abstract

Introduction

Conclusions

References

Tables

Figures

◀

▶

◀

▶

Back

Close

Full Screen / Esc

Printer-friendly Version

Interactive Discussion



Remotely sensed land-surface energy fluxes

R. Guzinski et al.

[Title Page](#)

[Abstract](#)

[Introduction](#)

[Conclusions](#)

[References](#)

[Tables](#)

[Figures](#)

◀

▶

◀

▶

[Back](#)

[Close](#)

[Full Screen / Esc](#)

[Printer-friendly Version](#)

[Interactive Discussion](#)



Table 4. ERA Interim meteorological inputs – statistical comparison of modeled vs. measured sensible heat flux at VOU for the three approaches used to estimate the constant ratio used during the disaggregation procedure and for the non-disaggregated high, ND_H , and low, ND_L , resolution fluxes. The statistical parameters used are bias (modeled–measured), root mean square error (RMSE), coefficient of variation (CV – RMSE divided by mean of observed values), and correlation (r). Bias and RMSE are in Wm^{-2} , the other parameters are unitless.

		EF	ND_H	ND_L
Bias	S75	2	–30	21
	S100	1	–10	22
RMSE	S75	60	76	78
	S100	18	58	47
CV	S75	0.39	0.48	0.50
	S100	0.11	0.37	0.30
r	S75	0.69	0.66	0.45
	S100	0.96	0.77	0.45

Remotely sensed land-surface energy fluxes

R. Guzinski et al.

Title Page

Abstract

Introduction

Conclusions

References

Tables

Figures

◀

▶

◀

▶

Back

Close

Full Screen / Esc

Printer-friendly Version

Interactive Discussion



Table 5. ERA Interim meteorological inputs – statistical comparison of modeled vs. measured sensible heat flux at GLU for the three approaches used to estimate the constant ratio used during the disaggregation procedure and for the non-disaggregated high, ND_H , and low, ND_L , resolution fluxes. The statistical parameters used are bias (modeled–measured), root mean square error (RMSE), coefficient of variation (CV – RMSE divided by mean of observed values), and correlation (r). Bias and RMSE are in Wm^{-2} , the other parameters are unitless.

		EF	ND_H	ND_L
Bias	S75	37	–193	76
	S100	20	–187	77
RMSE	S75	85	212	102
	S100	89	206	97
CV	S75	0.26	0.65	0.30
	S100	0.26	0.61	0.28
r	S75	0.74	0.63	0.78
	S100	0.56	0.60	0.80

BGD

11, 4857–4908, 2014

Remotely sensed land-surface energy fluxes

R. Guzinski et al.



Fig. 1. The two flux towers used for evaluating the model performance: Voulund (VOU, **a**), and Gludsted (GLU, **b**). The grid indicates the location of MODIS pixels in MODIS sinusoidal projection and the red plume originates from the location of the flux tower and illustrates a typical example of a flux measurement footprint of the EC system mounted on each of the towers.

[Title Page](#)[Abstract](#)[Introduction](#)[Conclusions](#)[References](#)[Tables](#)[Figures](#)[◀](#)[▶](#)[◀](#)[▶](#)[Back](#)[Close](#)[Full Screen / Esc](#)[Printer-friendly Version](#)[Interactive Discussion](#)

Remotely sensed
land-surface energy
fluxes

R. Guzinski et al.

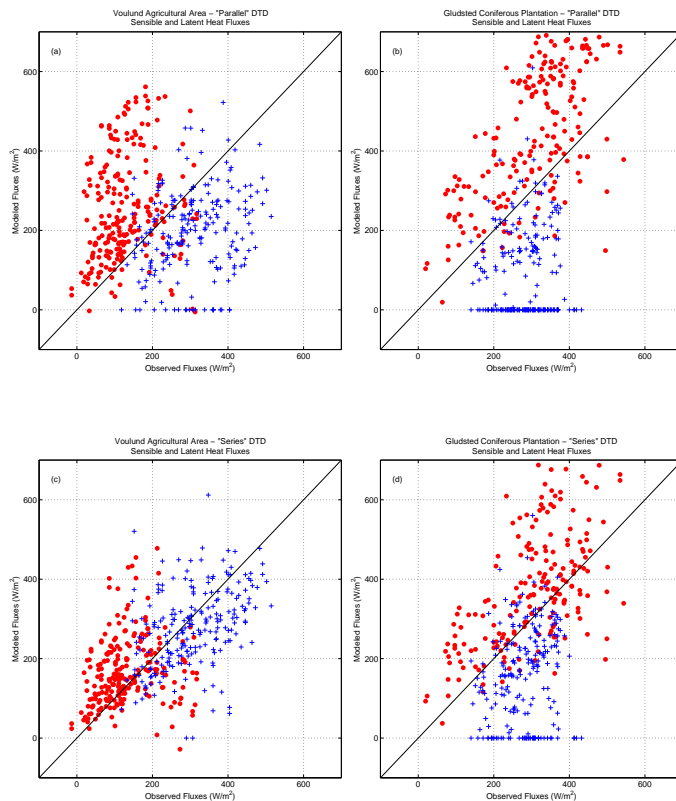


Fig. 2. Sensible heat (red dots) and latent heat (blue crosses) fluxes estimated over the period 2009–2013 with the DTD model over the Voulund agricultural area, panels (a) and (c), and Gludsted coniferous plantation, panels (b) and (d). The satellite input taken from 930 m resolution MODIS instrument on board Terra and Aqua satellites. In the top panels the “parallel” implementation of DTD was used, in the lower panels the “series” implementation.

[Title Page](#)[Abstract](#)[Introduction](#)[Conclusions](#)[References](#)[Tables](#)[Figures](#)[◀](#)[▶](#)[◀](#)[▶](#)[Back](#)[Close](#)[Full Screen / Esc](#)[Printer-friendly Version](#)[Interactive Discussion](#)

Remotely sensed
land-surface energy
fluxes

R. Guzinski et al.

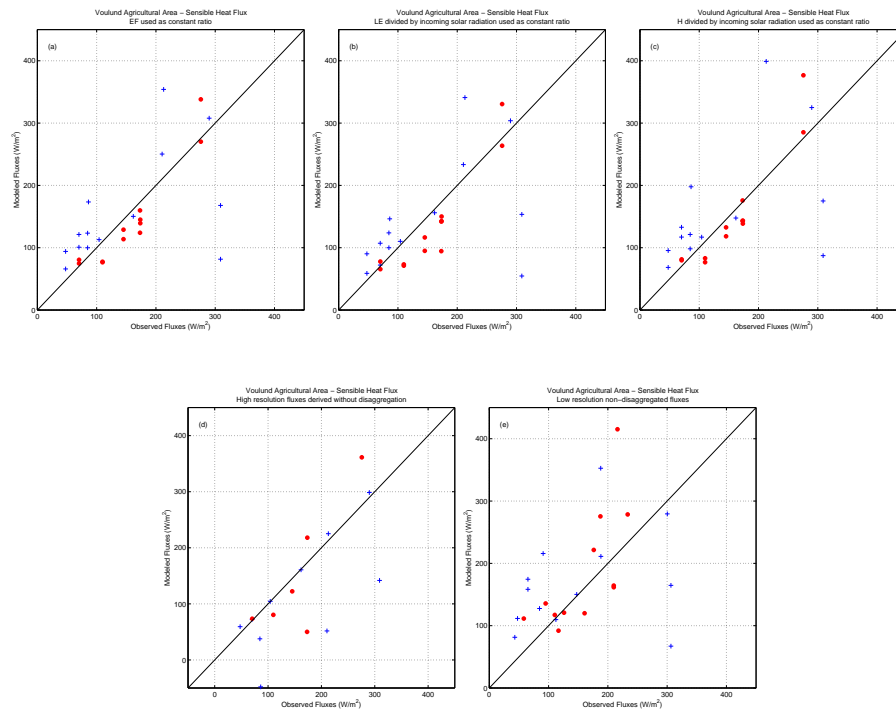


Fig. 3. Comparison of modeled and EC measured fluxes at the Voulund agricultural area. The three approaches used for determining the constant ratio during the disaggregation are: **(a)** evaporative fraction, **(b)** $LE/R_{s, in}$, **(c)** $H/R_{s, in}$. Panel **(d)** shows high resolution fluxes derived with TSEB model without disaggregation. The modeled fluxes in those panels are 30 m fluxes aggregated to EC footprint. Panel **(e)** shows the low resolution, non-disaggregated fluxes modeled with DTD. Crosses indicate aggregated fluxes where pixels comprising 75 % of EC footprint were present, circles where in addition there were no missing Landsat pixels within the MODIS pixels.

Title Page

Abstract

Introduction

Conclusions

References

Tables

Figures



Back

Close

Full Screen / Esc

Printer-friendly Version

Interactive Discussion



BGD

11, 4857–4908, 2014

Remotely sensed land-surface energy fluxes

R. Guzinski et al.



Fig. 4. Two examples of gaps present in the disaggregated high resolution flux estimates. On the left stripped gaps at VOU due to the failure of the sensor on board Landsat 7 and on the right gaps at GLU due to clouds during Landsat overpass. The darker reds indicate higher sensible heat fluxes. Even though small scale flux variations due to features such as roads or fields are properly modeled, the total heat flux within a MODIS pixel will be biased due to the gaps.

[Title Page](#)[Abstract](#)[Introduction](#)[Conclusions](#)[References](#)[Tables](#)[Figures](#)[◀](#)[▶](#)[◀](#)[▶](#)[Back](#)[Close](#)[Full Screen / Esc](#)[Printer-friendly Version](#)[Interactive Discussion](#)

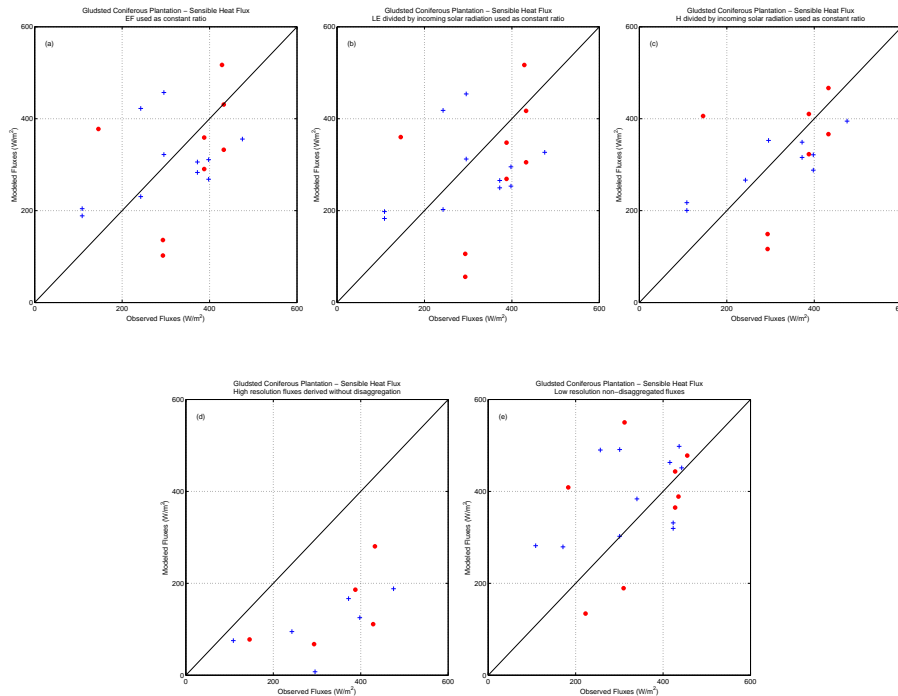


Fig. 5. Comparison of modeled and EC measured fluxes at the Gludsted coniferous plantation. The three approaches used for determining the constant ratio during the disaggregation are: **(a)** evaporative fraction, **(b)** $LE/R_{s, in}$, **(c)** $H/R_{s, in}$. Panel **(d)** shows high resolution fluxes derived with TSEB model without disaggregation. The modeled fluxes in those panels are 30 m fluxes aggregated to EC footprint. Panel **(e)** shows the low resolution, non-disaggregated fluxes modeled with DTD. Crosses indicate aggregated fluxes where pixels comprising 75 % of EC footprint were present, circles where in addition there were no missing Landsat pixels within the MODIS pixels.

Remotely sensed land-surface energy fluxes

R. Guzinski et al.

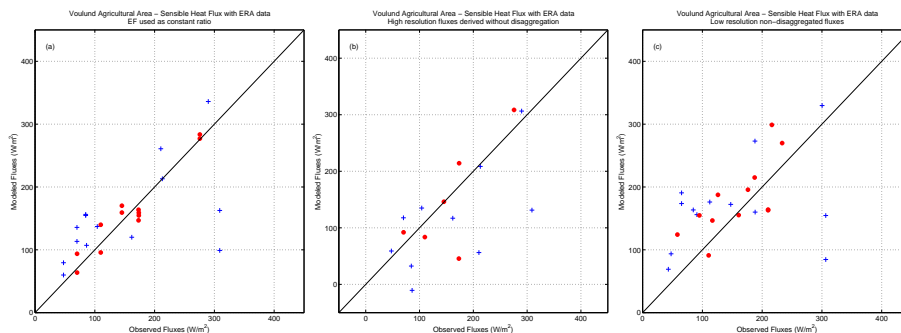


Fig. 6. Comparison of modeled and EC measured fluxes at the Voulund agricultural area with meteorological inputs provided by ERA Interim data set. The three panels show: **(a)** fluxes disaggregated using the evaporative fraction method, **(b)** high resolution fluxes derived with TSEB model without disaggregation, **(c)** low resolution, non-disaggregated fluxes modeled with DTD. The fluxes modeled at 30 m resolution **(a and b)** are aggregated to EC footprint. Crosses indicate aggregated fluxes where pixels comprising 75 % of EC footprint were present, circles where in addition there were no missing Landsat pixels within the MODIS pixels.

Title Page

Abstract

Introduction

Conclusions

References

Tables

Figures

◀

▶

◀

▶

Back

Close

Full Screen / Esc

Printer-friendly Version

Interactive Discussion



Remotely sensed land-surface energy fluxes

R. Guzinski et al.

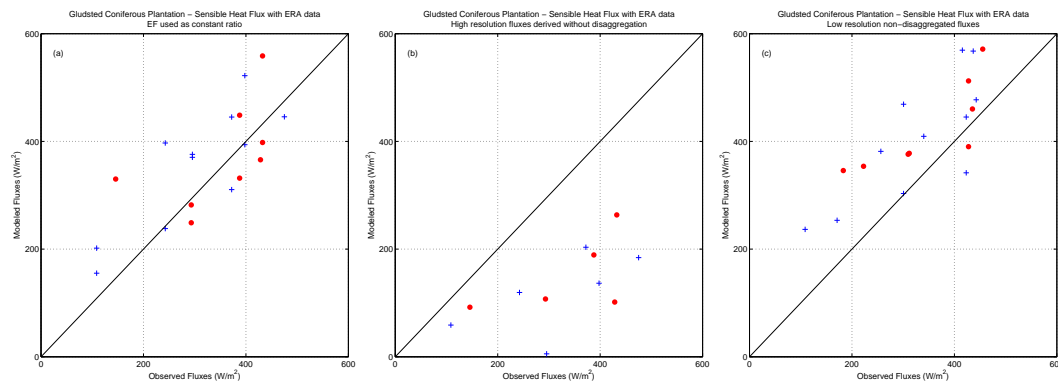


Fig. 7. Comparison of modeled and EC measured fluxes at the Gludsted coniferous plantation with meteorological inputs provided by ERA Interim data set. The three panels show: **(a)** fluxes disaggregated using the evaporative fraction method, **(b)** high resolution fluxes derived with TSEB model without disaggregation, **(c)** low resolution, non-disaggregated fluxes modeled with DTD. The fluxes modeled at 30 m resolution (panels **(a)** and **(b)**) are aggregated to EC footprint. Crosses indicate aggregated fluxes where pixels comprising 75 % of EC footprint were present, circles where in addition there were no missing Landsat pixels within the MODIS pixels.

[Title Page](#)
[Abstract](#)
[Introduction](#)
[Conclusions](#)
[References](#)
[Tables](#)
[Figures](#)
[⏪](#)
[⏩](#)
[◀](#)
[▶](#)
[Back](#)
[Close](#)
[Full Screen / Esc](#)
[Printer-friendly Version](#)
[Interactive Discussion](#)
